Spontaneous Raman Scattering Measurements and CFD Simulations of Major Species and Temperature in a Turbulent Dilute Hydrogen Diffusion Flame

Joseph A. Ranalli[1] and Peter Strakey[2]
National Energy Technology Laboratory, Morgantown, WV 26507

Dilute hydrogen diffusion flames represent a possible practical configuration for achieving extremely low emission of Nitric Oxides (NOx), and provide a challenging computational problem due to their complex turbulence-chemistry interactions and molecular transport effects. Experimental measurements of spatially resolved major species concentration and temperature were made in a hydrogen dilute diffusion flame using Spontaneous Raman Scattering, providing insight into the physical mechanisms leading to reductions in NOx and data for computational validation. Results from a computational model using Large Eddy Simulation (LES) were able to correctly predict several important flame features, such as the importance of differential diffusion effects in flame anchoring. Depressed flame temperatures were measured, resulting from the highly strained flame environment, providing a supporting explanation for the low NOx levels reported for this type of flame in the literature. The complex mechanisms governing the behavior of this flame make it an interesting target for computational validation.

Nomenclature

S_i	=	scattering intensity for species *i*
C	=	cross-talk calibration matrix
T	=	temperature
N	=	number density
x	=	mole fraction
f	=	mixture fraction
Z	=	elemental mass fraction
Φ	=	equivalence ratio
T_{ad}	=	adiabatic flame temperature
T_{corr}	=	flame temperature corrected for heat loss to the calibration burner surface

I. Introduction

IN an increasingly carbon-constrained world, safe and clean combustion of high-hydrogen fuels is becoming a pertinent research area in the gas turbine community. The U.S. Department of Energy has a significant research effort underway through its Integrated Gasification Combined Cycle (IGCC) program that is involved in near zero carbon emission power generation. The basic design is that of an IGCC plant with a water-gas shift reactor to convert the synthesis gas into hydrogen and carbon dioxide. After the CO_2 is separated from this mixture it is sequestered, leaving a high-hydrogen fuel to be burned in the gas turbine. Due to the potentially troublesome prospect of premixing hydrogen and air for combustion in the gas turbine, the current work is exploring the feasibility of utilizing diffusion flames in the combustor, where the hydrogen can be diluted with about 50% nitrogen by volume, available from the coal gasifier's air separation unit, to help control the combustion temperature.

[1] Postdoctoral Research Associate, Member AIAA, joseph.ranalli@or.netl.doe.gov
[2] Research Scientist, Member AIAA, peter.strakey@netl.doe.gov

Even with a 50/50 H_2/N_2 fuel mixture, adiabatic flame temperatures are too high (~2025 K) to fully suppress NO_x formation, thus additional strategies must be employed to meet the DOE Turbine Program's goal of 2 ppm NO_x @ 15% O_2. The primary NO_x reduction strategy investigated in this work is the reduction of the flame residence time and flame temperature, which is accomplished by using small, highly strained nitrogen-diluted diffusion flames. This approach has been studied extensively at NETL over the past several years in both atmospheric pressure burners and high-pressure combustors[1-6]. The results indicate that NOx emissions can easily be reduced to less than 10 ppmv @ 15%O2 at realisitic gas turbine pressures and firing temperatures with reasonable injector pressure drop. The optimization of the injector involves a tradeoff between NOx emissions, pressure drop and flame stability.

Flame strain is induced by relatively high injection velocities (100-200 m/s) which can create flame stabilization issues, and is an area of ongoing research[1]. A key factor in flame stabilization is preferential diffusion in which hydrogen diffuses into the surrounding air stream faster than the nitrogen diluent creating localized regions of higher equivalence ratio. Some of the previous experimental studies were accompanied by Computational Fluid Dynamics (CFD) studies that showed some promise in predicting trends in NOx emissions as a function of injector geometry and operating conditions[2]. This flame environment has been found to be a challenging problem for computational modeling due to the complex turbulence-chemistry interactions as well as molecular transport effects. The importance of accurate computational modeling is to provide deeper insight into the complex physical and chemical phenomena that govern flame stability and NOx formation. However, in order to ensure the fidelity of such computational models, substantial experimental validation is required.

While data such as global NOx emissions, blowoff point and flame length provide valuable information for practical design purposes, more detailed data is needed to validate computational tools. Non-intrusive laser diagnostic techniques such as Coherent Anti-Stokes Raman Spectroscopy (CARS) and Spontaneous Raman Scattering (SRS) have been used for many years now to provide spatially and temporally resolved measurements of major species and temperature and are relatively mature diagnostic techniques[2]. The approach taken in this study involves SRS line-imaging of the major species and temperature using a high power YAG laser and a highly efficient CCD based detection system.

This technique provides radial profiles of instantaneous temperature and major species which can be directly compared to modeling results. In an effort to test the capability of commercially available CFD codes, a Large Eddy Simulation (LES) using the FLUENT code was conducted at one operating condition. The results of the experimental measurements as well as the LES results are presented here.

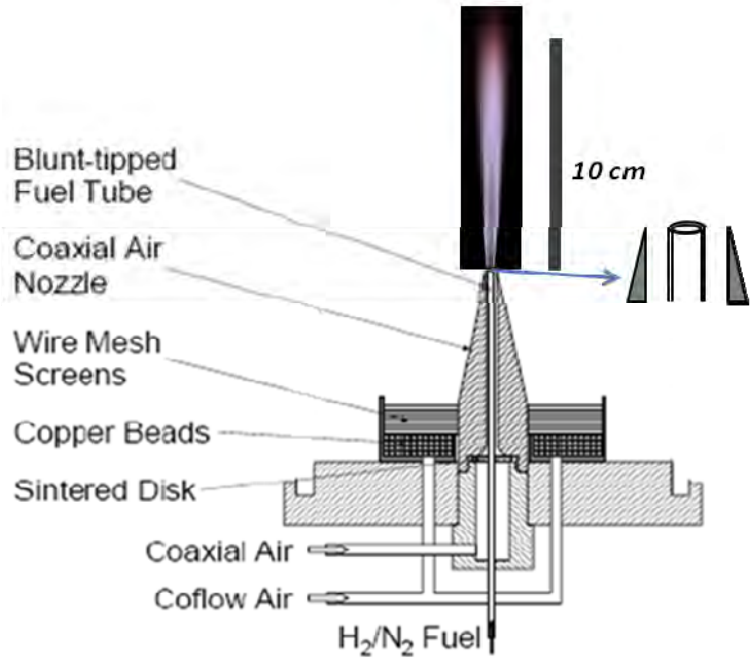

Fig. 1. Schematic of the burner with a typical flame image.

II. Experimental System

A. Burner Configuration

The burner used in this study is similar to that described in Ref. [1]. The burner consists of a stainless steel tube which delivers a fuel jet. Surrounding the fuel jet is a region of high velocity coaxial air delivered at an equivalence ratio of Φ =0.50. A surrounding co-flow of air is supplied to over-ventilate the flame with an overall equivalence ratio of 0.2. The burner is enclosed in a Pyrex tube to allow global emissions measurements to be made. A schematic of the burner with a typical visible image of the flame is shown in Fig. 1. Fig. 2 shows NOx emissions corrected to 15% O2 as a function of coaxial air velocity for several different fuel jet velocities and air annulus diameters. For the SRS measurements in this

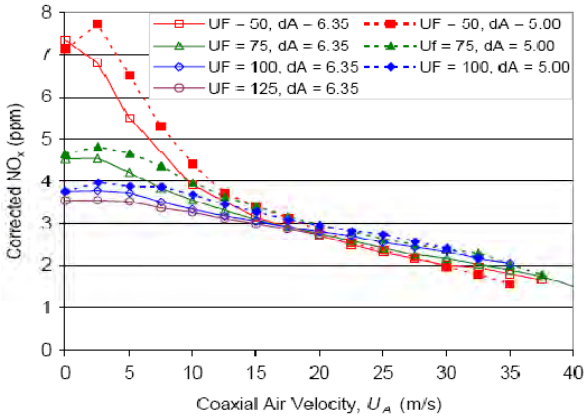

Fig. 2. NOx emissions corrected to 15% O_2 as a function of coaxial air velocity for several fuel velocities and air annulus diameters.

study, a single operating condition was used. For the experimental measurements made here, the fuel jet diameter was 2.118 mm in diameter and the coaxial air jet was 6.35 mm in diameter. A fuel composition of 50% H2 with 50% nitrogen by volume was delivered at a total flow rate of 15.45 slpm, corresponding to a fuel jet velocity of approximately 75 m/s. The coaxial air velocity was 27 m/s. Due to the high laser power used in the measurements, the Pyrex enclosure was removed to prevent multi-photon ionization breakdown of the glass material. Because the flame is over-ventilated by the surrounding co-flow air, removal of the enclosure was found to have little or no effect on the structure of the flame.

B. Raman Spectroscopy System

The laser used for the Raman scattering measurements was a frequency-doubled Nd: YAG emitting 1000mJ/10ns pulses at the 532 nm line. The high energy level necessitated use of an optical pulse stretcher to reduce the peak power focused into the probe volume. The design for the pulse stretcher was similar to a 3-cavity stretcher described by Kojima and Nguyen[7], with the main exception that the cavity lengths were used in order of shortest to longest to reduce clipping due to beam divergence. A sketch of the pulse stretcher arrangement as found in the optical train is found in Fig. 3. The pulse stretcher reduced the peak power of the laser beam by a factor of ten and eliminated multi-photon ionization breakdown of the gasses at the probe volume. The resultant beam had an intensity of around 900mJ over 100ns. The beam from the pulse stretcher was focused into the probe volume at the burner with a 750 mm focal length lens. A mirror was used to reflect the laser beam back through a 400 mm focal length lens resulting in two passes of the laser beam through the flame thus doubling the effective laser power. The reflected beam was offset slightly in the horizontal direction to reduce the peak laser power at the probe volume and prevent optical breakdown of the gasses. The resulting elliptical probe volume was approximately 120 μm high by 240 μm deep. Part of the incident beam was split onto a separate camera for alignment of the pulse stretcher and a photodiode for sensing of the shot-to-shot laser power variation using a box-car integrator.

The light from the probe volume was collected by a pair of *f*2.0 achromat lenses and focused into a *f*1.8 transmission spectrometer. The spectrometer contained a holographic notch filter to remove the Rayleigh line. The output of the spectrometer was imaged by a cooled CCD camera (Pixis 2048). The holographic transmission grating used in the spectrometer allowed for full capture of the entire visible spectrum from 400 nm to 700 nm, allowing both Stokes and anti-Stokes spectra to be captured. The system imaged a 16 mm segment of the laser beam, resulting in images in which the vertical dimension represents distance along the imaging line and the horizontal dimension is wavelength. The line imaging approach employed here allowed for single shot radial profiles of major species and temperature. Binning of the images by 8 pixels in the spatial dimension and 4 pixels in the spectral dimension was used to improve the signal-to-noise ratio while still allowing a resolution of about 0.6 nm in the spectral direction and 107 μm spatially along the path of the laser beam. Despite the fact that the experiment was performed with the room lights off, some stray light as well as flame chemiluminescence occurred in the background of the images. A custom mechanical shutter made from a hard-drive actuator and a commercial beam chopper were used together to limit the time during which the CCD array was exposed to approximately 120 μsec, reducing the background signal to an acceptable level.

C. OH PLIF System

OH PLIF measurements were made in order to directly compare the flame length and heat release distribution to the LES results.The OH-PLIF system consisted of a Spectra Physics Nd:YAG laser, PDL-1 dye laser and doubling crystal to produce ~10 nsec laser pulses at 10 Hz with about 30 mJ of output per pulse at the Q1(9) line of the (1,0) band of the OH $A^2\Sigma - X^2\Pi$ electronic transition at 283.92 nm. This particular line was selected because it is one of the strongest transitions and has only a mild temperature dependence over the ranges of temperatures expected here.

A combination of fused silica cylindrical and spherical lenses was used to form a laser sheet approximately 125 mm high and 200 μm thick, which was directed through the center of the combustor. A Princeton Instruments PI

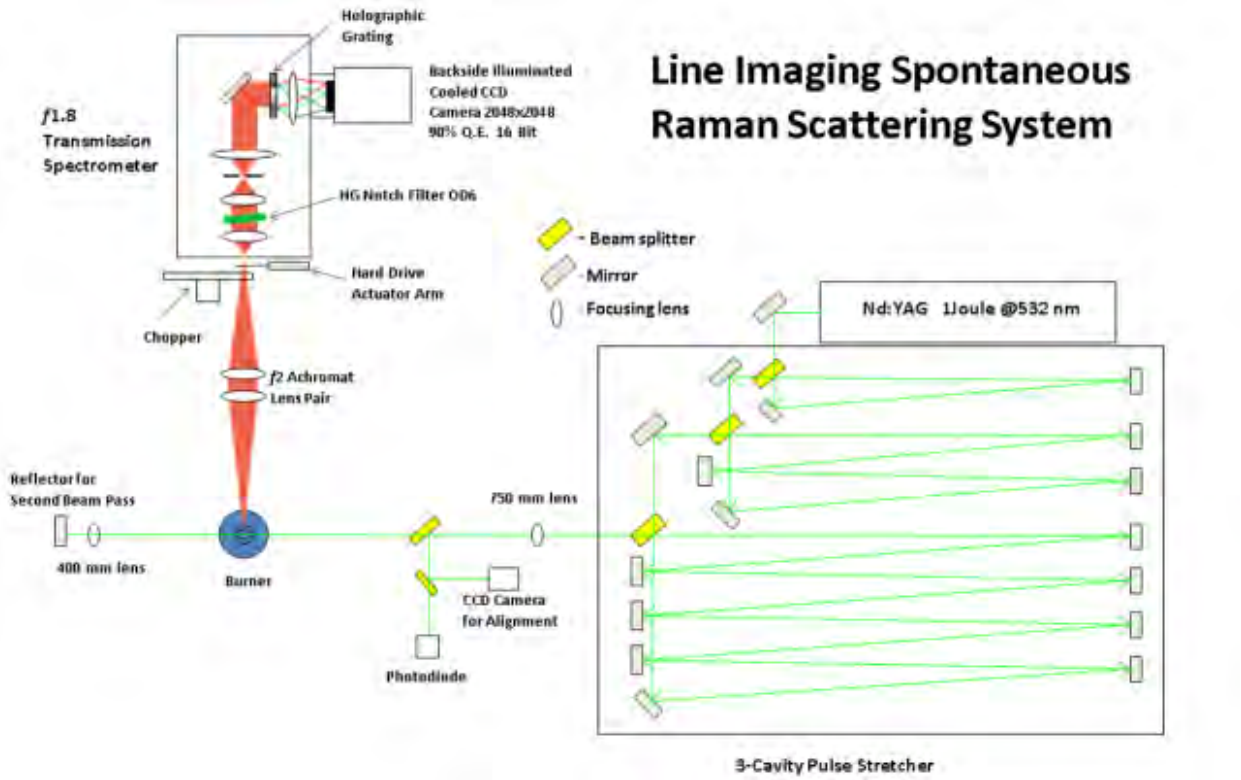

Fig. 3. Top view sketch of the experimental setup

Max intensified camera with a 1024 x 1024 sensor and a 45 mm *f*1.8 fused silica lens with both long-pass and band-pass filters was used to image the fluorescence signal around 310 nm while blocking most of the unwanted scattered laser light.

D. Raman System Calibration

In order to make quantitative measurements of the major species in the flame, it was necessary to calibrate the Raman system in a known flame environment. For this purpose, the hydrogen burner was replaced with a laminar McKenna flat-flame burner and a set of calibration spectra were acquired. This type of burner has been well characterized in the literature as a calibration source for temperature and equilibrium species[8]. Since this burner type is not adiabatic, an effort was made to reduce the effects of heat losses by keeping their value to less than 10% of the total heat release. In addition, flame temperatures and species concentrations were corrected for heat loss by measuring the temperature rise in the water used to cool the burner surface.

The calibration methodology for Raman signals was based on the crosstalk calibration matrix described by Dibble *et al.*[9] In this formulation, we can consider that the Raman signal for a specie S_i can be written as the sum of the contributions of all species within the wavelength considered for specie i:

$$S_i = \sum_j C_{i,j}(T) N_j = \sum_j C_{i,j}(T) \frac{x_j}{T} \tag{1}$$

The matrix $C(T)$ is termed the crosstalk matrix, and accounts for the crosstalk of all species j onto the wavelengths of specie i, and has a dependence on temperature. This equation can be inverted using an iterative process on temperature to compute the mole fractions x_j from the measured intensities. The temperature can be obtained either through the ideal gas law (i.e. iterating on the theoretical total molecular density) or via the Stokes/anti-Stokes ratio of the Nitrogen Raman scattering.

The actual values for the elements of the crosstalk matrix are dependent on the optical characteristics of the system in question, as well as the wavelengths considered to represent each species. In this case, spectral binning

Table 1. Superpixel wavelengths used for each species, including that for Anti-Stokes Nitrogen

Species	Wavelengths (nm)
N_2	600-613
O_2	574-584
H_2O	650-665
H_2	678-688
N_2 (AS)	467-483

Table 2. Summary of calibration flame conditions

Flame	Φ	%N_2	T_{ad}(K)	T_{corr}(K)
1	0.4	0	1427	1402
2	0.74	0	2078	1968
3	1.7	6	2070	1757
4	3.0	25.6	1409	1329
5	4.0	42.7	1034	943

was used to sum over each species' main peak, yielding spectral "superpixels" that represent a single intensity value for each species. The wavelengths used as the left and right boundaries for each superpixel are given in Table 1.

As a practical matter in computation of the crosstalk terms, judicious selection of operating conditions was used to reduce the number of species present in the flame at any one time. For example, by running lean, hydrogen could be eliminated in the equilibrium region; likewise oxygen can be eliminated in rich flames. For the given setup and over the specified wavelengths, the only crosstalk which was found to be significant was that of the rotational hydrogen lines onto oxygen. This effect can be seen in the example calibration spectrum in Fig. 4. The resultant crosstalk matrix can be written as:

$$C(T)=\begin{bmatrix} c_{N2}(T) & 0 & 0 & 0 \\ 0 & c_{O2}(T) & 0 & c_{H2\to O2}(T) \\ 0 & 0 & c_{H2O}(T) & 0 \\ 0 & 0 & 0 & c_{H2}(T) \end{bmatrix} \tag{2}$$

The temperature dependencies of the calibration matrix terms were determined by conducting the calibration experiment at several flame temperatures. A summary of these flame operating conditions is found in Table 2. As stated previously, hydrogen and oxygen are not present together in any of the calibration flames. In addition, room temperature calibrations were obtained in a non-reacting case for the reactant gases. The temperature dependence of the calibration matrix elements may be found in Fig. 5 and are compared with scaled fits of theoretical predictions made using RAMSES[10]. In addition to computation of the calibration matrix, the calibration procedure also allowed an experimental calibration of the nitrogen Stokes/Anti-Stokes ratio temperature measurement across the range of flame temperatures tested. In both the case of the calibration matrix and the nitrogen S/AS temperature, polynomial

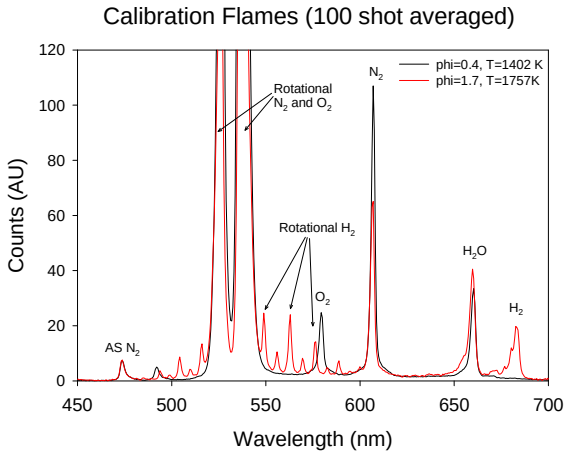

Fig. 4. Sample spectra from the calibration burner operating on hydrogen.

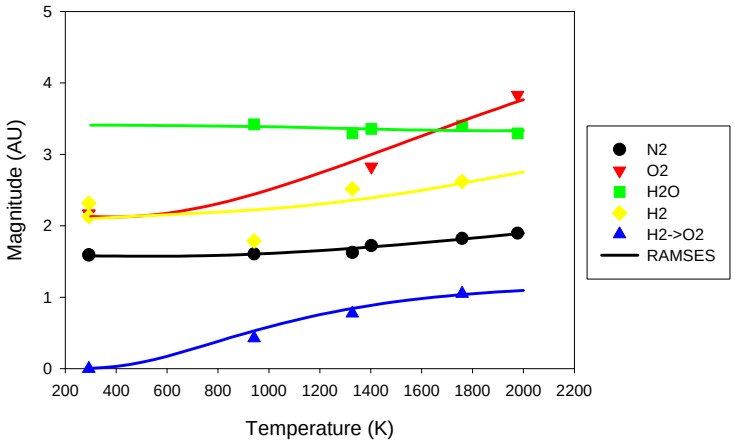

Fig. 5. Calibration matrix element measurements as a function of temperature, compared with scaled and offset fits of the crosstalk behavior computed from RAMSES[10].

curve fits to the experimental data were used to provide the necessary temperature functionality.

In addition to application of the calibration, some additional processing on the images was necessary to correct two effects introduced by the optical system. The effect of slit curvature introduced a spatial dependence in the pixel-to-wavelength calibration and optical vignetting caused non-uniformities in the baseline intensity in the spatial dimension. Correction of both of these effects was accomplished by measuring a uniform room air spectrum prior to each test. This allowed the slit curvature effect to be removed by applying a spatially dependent wavelength calibration based on the expected locations of the nitrogen and oxygen peaks at room temperature conditions. Vignetting was corrected by normalizing the room air superpixel intensities to result in a uniform spatial profile.

E. Computational Studies

Simulations on the target flame were carried out with the commercial CFD code FLUENT using the Large Eddy Simulation (LES) approach. The chemical mechanism used here was the detailed hydrogen-air kinetic mechanism of Li *et al.*[11] For the LES studies, a 3D unstructured grid of approximately 3 million cells was used. The computational domain extended 10 cm upstream into the fuel and air tubes to accurately predict the flowfield exiting the fuel and air tubes. Mass flowrate boundary conditions were used for the inlets with a spectral synthesizer method to prescribe turbulent fluctuations on the mean inlet velocity. The bottom and sides of the computational domain were prescribed as pressure inlets. The top of the domain was a pressure outlet boundary condition.

No turbulence-chemistry interaction model was used for the LES studies, which is the equivalent of assuming that the sub-grid scalars were perfectly mixed. This is somewhat justified considering the high resolution of the grid, which was approximately 100 μm in the reaction zone, and the fast molecular mixing time-scale of hydrogen. A dynamic Smagorinsky model was used to calculate the sub-grid turbulent viscosity. A mixture averaged molecular transport approach was taken using kinetic theory to calculate the mass diffusion coefficients of the individual species. Central differencing was used for the momentum equations while 2nd urder upwinding was used for the scalars. The temporal discretization was 2nd order and a maximum CFL number of 0.7 was used for the time step. The domain for the LES simulations was initialized using a RANS calculation and the simulations were run until the RANS solution was flushed out and a statistically steady-state solution was achieved.

III. Results

A sample single-shot Raman spectrum image is shown in Fig. 6. The vertical dimension in the figure corresponds to the spatial dimension of the diagnostic, while the horizontal dimension is the spectrum. Scattering from each of the major species in the flame is clearly visible. The various regions in the diffusion flame are evident; a central region contains hydrogen and nitrogen with air (oxygen and nitrogen) present in the outer region. Water is visible in reaction zone (the interface between the two), along with increased anti-stokes scattering from nitrogen indicating higher temperatures in the flame. Applying the image conditioning and superpixel binning described above to images such as this then allows calculation of the individual species concentrations as a function of radial distance.

Ensemble averaged species concentrations and temperature from the Raman measurements were obtained by averaging 200 individual measurements and the radial profiles were then averaged about the centerline of the profile. The species and temperature profiles at several axial locations are shown in Fig. 7. The Raman measurements were able to very accurately reproduce the known species concentration values in the unmixed fuel and air regions. Experimental species concentration RMS variations in these known regions was around 1.5% of the mean, depending on the specie being considered. Temperature RMS values reached approximately 10% of the mean at the peak of the temperature profile. In contrast, at the furthest downstream location, the RMS temperature associated with the peak was around 35% of the mean temperature value. The flame region is observed to be quite thin near to the burner surface, having a reaction region width less than 1mm, and was comparatively steady as indicated by these RMS measurements. This feature can also be observed qualitatively considering the instantaneous LES simulation results, as in Fig. 8. The core fuel region remains basically undisturbed on the centerline until reaching the 15.5mm axial location.

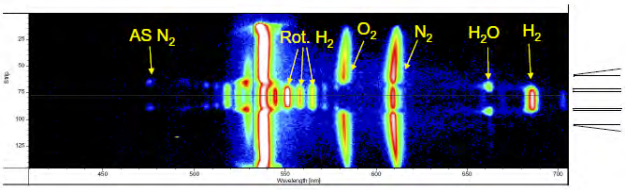

Fig. 6. Sample raw Raman spectrum taken approximately 2mm above the burner tip. The horizontal axis is wavelength and the vertical axis is radial distance. Note that the effects of vignetting and slit curvature are still visible.

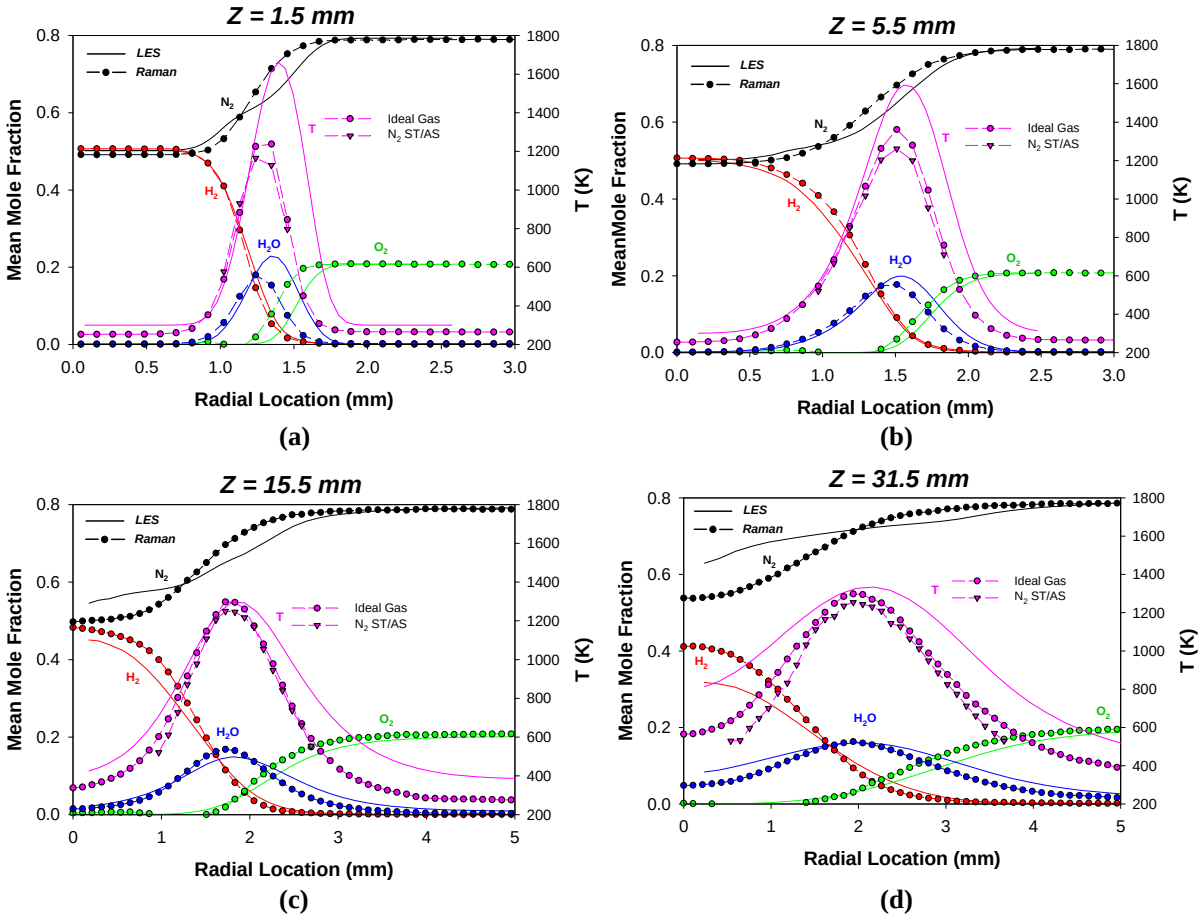

Fig. 7. Comparison of ensemble averaged species concentration and temperature for Raman measurements and LES predictions. Measurements are averaged to provide radial profile. Results shown at four separate heights above the burner tip.

The temperatures predicted by the ideal gas law and the nitrogen Stokes/Anti-Stokes (N_2 S/AS) ratio are in reasonably good agreement. The ideal gas law predicts higher temperature values, consistent with the neglect of minor species in the ideal gas law approach. Measurements of N_2 S/AS are limited by noise at low temperatures due to reduced AS intensity. For both temperature calculations, the highest peak temperature was observed slightly downstream at the 5.5mm axial location. This is consistent with observations of the reaction region position made by Weiland et al.[3] for cases with a high coaxial air velocity. The peak temperatures observed were around 1300 K and are well below adiabatic flame temperatures for this flame (~2025 K). In order to determine if a flamelet could even be sustained at these relatively low temperatures, a simple model of opposed jet diffusion flames for this fuel and air condition was run in CHEMKIN using the OPPDIFF code. The hydrogen-air mechanism of Li et al[11] was used with a 50/50 hydrogen nitrogen mixture entering on one side and air on the opposing side. The velocities were kept equal and gradually ramped up to increase the strain rate until flame extinction occurred. The resulting

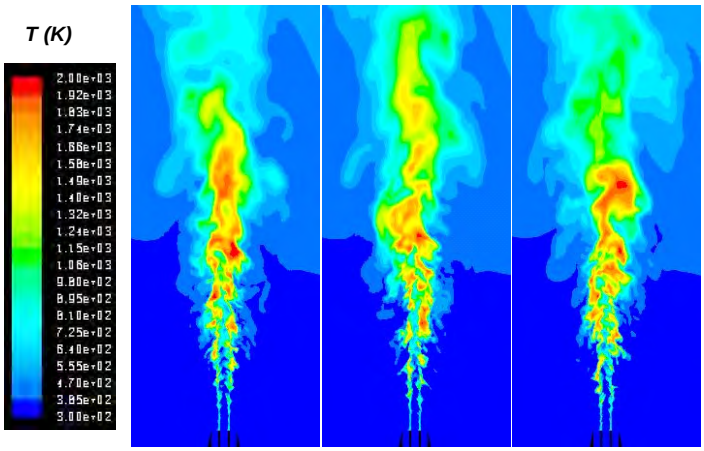

Fig. 8. Three instantaneous snapshots of the temperature field from the LES simulations.

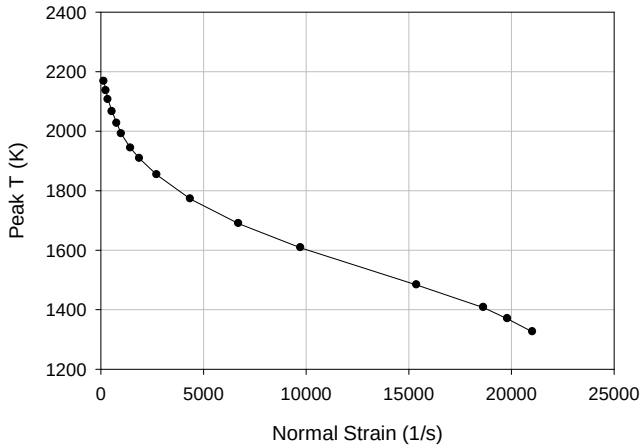

Fig. 9. Temperature vs. strain rate for a opposed jet flame model run in CHEMKIN

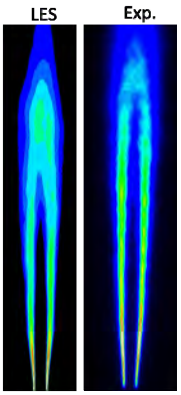

Fig. 10. Comparison of averaged OH concentration from LES and OH PLIF measurements. Note that the experimental values are normalized and no calibration has been applied.

relationship between normal flame strain and peak flame temperature is shown in Fig. 9. The flame temperatures measured for this flame are near the strain extinction limit predicted by this model, but do show that temperatures of 1300K are sufficient to sustain the diffusion flame These relatively low peak flame temperatures also help to explain the extremely low NOx values observed for this flame (~ 2ppm[3]).

Three instantaneous snapshots of the temperature field from the LES simulation is shown in Fig. 8. The snapshots show that there is very little fluctutation in the temperature field near the flame with a "laminar-like" appearance. The high strain rate induced in the shear layer does however produce large fluctuations in the flame further downstream.

The time-averaged radial profiles from the LES results, which are plotted in Fig. 7 consistently show a higher time-averaged peak flame temperature than the measurements. This is especially evident close to the burner surface. This is likely due to the use of a laminar chemistry approach which neglects turbulence-chemistry interactions by assuming infinitely fast mixing at the sub-grid scale. At downstream axial locations, better agreement is found for the peak temperature, but the amount of flame spreading is significantly over-predicted, resulting in a much broader temperature profile than seen in the measurements. These over-predictions are most likely due to over-prediction of the turbulence level in the inlet fuel tube, resulting in increased mixing. This effect is somewhat reduced at higher axial locations, except along the centerline, where measurements indicate that the core flow breaks up more slowly than predicted. This can also be seen by comparing LES predictions of OH concentration with OH PLIF measurements in the flame. Figure 10 shows that the LES predicts a shorter overall flame brush than that measured with the OH PLIF. These results are consistent with the over-prediction of mixing found in the species profiles.

It is interesting to note that differential diffusion of hydrogen plays an important role in flame stabilization. In the LES simulations, when the unity Lewis number assumption was applied, the flame would not stabilize on the rim of the fuel tube and simply blew off. Only when variable species diffusion was applied in the simulations would the flame stabilize on the fuel tube.

The occurrence of differential diffusion can be observed by looking for the presence of superadiabatic flame temperatures as a function of mixture fraction. Mixture fraction is defined as:

$$f_i = \frac{Z_i - Z_{i,coax}}{Z_{i,\,fuel} - Z_{i,coax}} \tag{3}$$

Here, Z_i represents the elemental mass fraction of either H or O atoms. In the absence of molecular transport effects, the mixture fraction based on either H or O atoms should be exactly equal. Fig. 11 shows plots of the temperature against mixture fraction for both the LES model prediction and the experimental data at several axial locations. The presence of superadiabatic temperatures in the oxygen mixture fraction plot (Fig 10(a)) is evidence of preferential diffusion low in the flame. This is observed both in the experimental data as well as the LES simulation. Note that the preferential diffusion effects are only observed in the experiment at low axial locations,

though they are present in the model to a small extent further downstream as well. This indicates that while preferential diffusion is important in flame anchoring, its effects are quickly overwhelmed by turbulent mixing.

IV. Conclusions

A diluted hydrogen diffusion flame was investigated using single-shot Raman spectroscopy diagnostics. The measurements were able to reveal spatially resolved major species and temperature profiles within the flame. Strongly depressed flame temperatures were observed resulting from the strained flame environment. These reduced temperatures provide an explanation for the reductions in NOx seen for this flame type in the literature. The flame was observed to anchor on the burner tip, providing relatively steady flame temperature and species profiles at upstream locations. Further downstream, the effects of turbulence began to dominate, resulting in significant unsteadiness in the distribution. Overall, the LES results were reasonable in comparison with the experimental data, but suggest that the modeling approach resulted in an over prediction of mixing, leading to an overly broad reaction zone. The simulation also over-precicted the peak flame temperature near the flame base, which is believed to be due to the modeling assumption of infinitely fast mixing at the sub-grid scale. The effects of preferential diffusion were observed in both experiments and computations near the burner tip, which are known to have a strong influence on anchoring in the CFD modeling results. The importance of these effects, along with the practical promise of low-NOx operation, makes this flame an interesting target flame for computational model validation. The validated CFD results will allow for improved insight into the complex physical and chemical processes that govern the important flame phenomena.

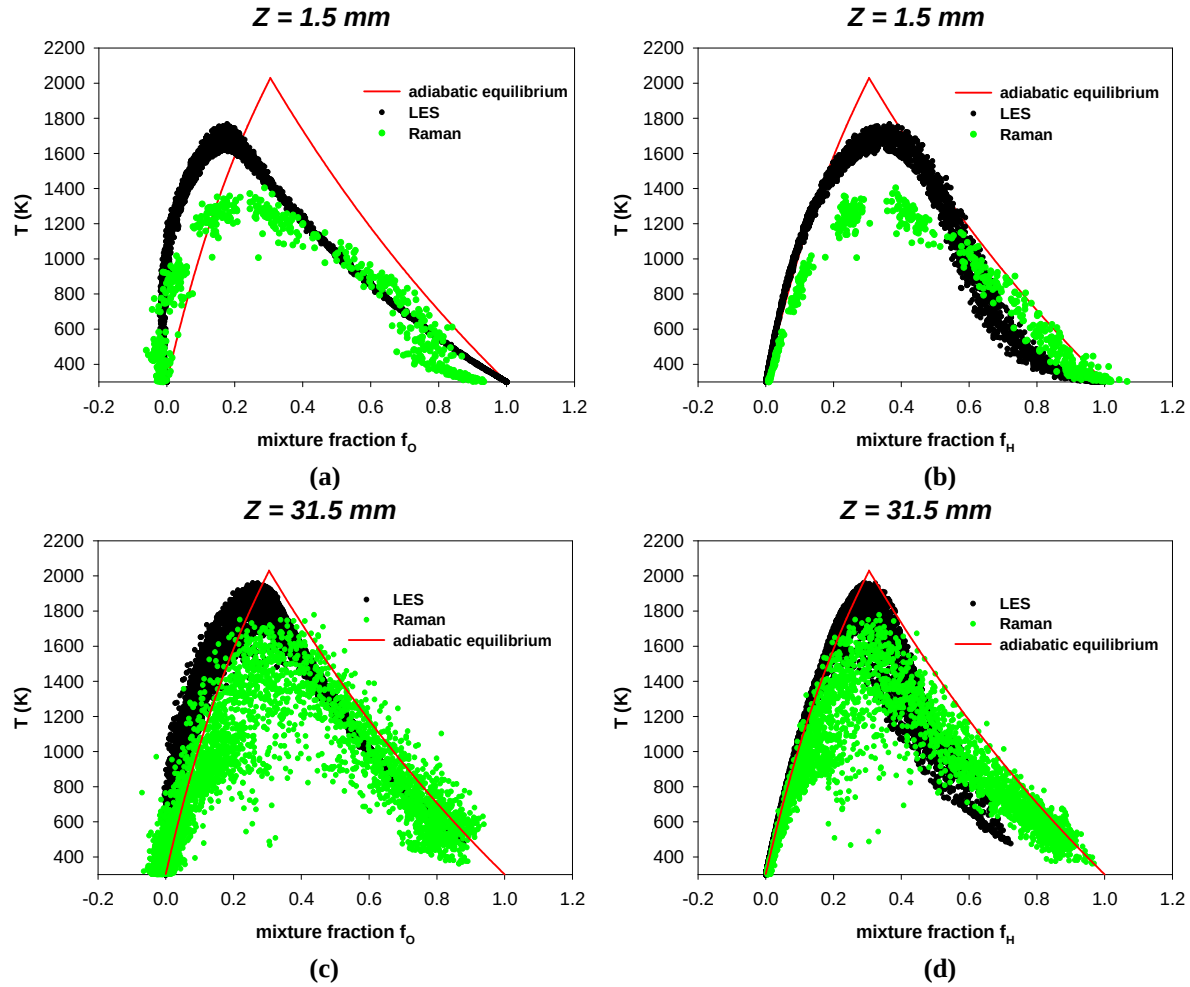

Fig. 11. Temperature vs. Mixture Fraction for both LES and Raman at two different axial locations.

Acknowledgments

The support of the U.S. DOE Turbines program and Advanced Research program is gratefully acknowledged. J. Ranalli gratefully acknowledges the support of the Oak Ridge Institute for Science and Education (ORISE) Postdoctoral Fellowship program.

References

[1]Weiland, N.; Strakey, P. "Stability Characteristics of Turbulent Hydrogen Dilute Diffusion Flames," *Combustion Science and Technology*, Vol. 181, 2009, pp. 756-781.

[2]Weiland, N. T.; Strakey, P. A. "NOx Reduction by Air-Side Versus Fuel-Side Dilution in Hydrogen Diffusion Flame Combustors," *J. Eng. Gas Turbines Power*, Vol. 132, 2010, 071504.

[3]Weiland, N.; Chen, R.; Strakey, P. "Effects of coaxial air on nitrogen-diluted hydrogen jet diffusion flame length and NOx emission," *Proceedings of the Combustion Institute In Press, Corrected Proof.*

[4]Weiland, N. T.; Strakey, P. A. "Stability Regimes of Turbulent Nitrogen-Diluted Hydrogen Jet Flames," In *Proceedings of the 5th US Combustion Meeting*, San Diego, CA, 2007.

[5]Weiland, N. T.; Strakey, P. A. "Global NOx Measurements in Turbulent Nitrogen-Diluted Hydrogen Jet Flames," In *Proceedings of the 5th US Combustion Meeting*, San Diego, CA, 2007.

[6]Weiland, N.; Sidwell, T.; Strakey, P. " Effect of Pressure and Air Preheating on Dilute Hydrogen Jet Diffusion Flames with Coaxial Air Injection," In *Proceedings of the 2010 Technical Meeting of the Central States Section of The Combustion Institute*; Central States Section/Combustion Institute: Champaign, IL, 2010.

[7]Kojima, J.; Nguyen, Q. "Laser Pulse-Stretching with Multiple Optical Ring Cavities," *Appl. Opt.*. Vol. 41, 2002, pp. 6360-6370.

[8]Sutton, G.; Levick, A.; Edwards, G.; Greenhalgh, D. "A combustion temperature and species standard for the calibration of laser diagnostic techniques," *Combustion and Flame*, Vol. 147, 2006, pp. 39-48.

[9]Dibble, R.; Starner, S.; Masri, A.; Barlow, R. "An Improved Method of Data Aquisition and Reduction for Laser Raman-Rayleigh and Fluorescence Scattering From Multispecies," *Applied Physics B-Photophysics and Laser Chemistry*, Vol. 51, 1990, pp. 39-43.

[10]Geyer, D. "1D-Raman/Rayleigh Experiments in a Turbulent Opposed-Jet," PhD Thesis, TU Darmstadt: Düsseldorf, Germany, 2005.

[11]Li, J.; Zhao, Z.; Kazakov, A.; Dryer, F. "An updated comprehensive kinetic model of hydrogen combustion," *International Journal of Chemical Kinetics*, Vol. 36, 2004, pp. 566-575.